Novel Gd-Substituted LiNi Ferrite/Polyaniline Composite Prepared by *In Situ* Polymerization

Jing Jiang,[1,2] Liangchao Li,[1] Feng Xu[1]

[1]*Zhejiang Key Laboratory for Reactive Chemistry on Solid Surface, Department of Chemistry, Zhejiang Normal University, Jinhua 321004, China*
[2]*School of Chemistry and Chemical Industry, China West Normal University, Nanchong 637002, China*

Received 14 April 2006; accepted 21 January 2007
DOI 10.1002/app.26156
Published online 6 April 2007 in Wiley InterScience (www.interscience.wiley.com).

ABSTRACT: Magnetic composite containing polyaniline (PANI)-coated $LiNi_{0.5}Gd_{0.08}Fe_{1.92}O_4$ was synthesized by *in situ* polymerization of aniline on the surface of $LiNi_{0.5}Gd_{0.08}Fe_{1.92}O_4$ ferrite particles. The obtained samples were characterized by powder X-ray diffraction, Fourier transform infrared spectra, UV–visible absorption spectra, thermogravimetric analysis, transmission electron microscopy (TEM), and vibrating sample magnetometer. The results of spectroanalysis indicated that there was interaction between PANI chains and ferrite particles. TEM study showed that composite presented the core–shell structure. The composite under applied magnetic field exhibited the clear hysteretic behavior at room temperature. The bonding mechanism in the composite had been discussed. © 2007 Wiley Periodicals, Inc. J Appl Polym Sci 105: 944–950, 2007

Key words: composite; polyaniline; ferrite; magnetic properties

INTRODUCTION

Conducting polymers have attracted considerable attention for their potential applications in various fields such as electromagnetic interference (EMI) shielding, rechargeable battery, electrodes and sensors, corrosion protection coatings, and microwave absorption.[1–5] Among the conducting polymers, polyaniline (PANI) has been extensively studied in the last two decades because of its unique electrochemical and physicochemical behavior, good environment stability, and relatively easy preparation.[6,7]

Conducting polymer–inorganic composites possess not only the nature of the flexibilities and processability of polymers, but also the mechanical strength and hardness of inorganic components. Recently, many interesting research has focused on the PANI-inorganic composites to obtain the materials with synergetic or complementary behavior between PANI and inorganic nanoparticles. Several reports on the synthesis of the composites of PANI with the inorganic nanoparticles such as oxide, sulfide, nitride, metal, and clay have been described.[8–12]

The soft magnetic Li—Ni ferrites have widely used in microwave devices, such as isolators, circulators, and phase shifters because of their dielectric and magnetic properties.[13,14] It is interesting to note that the electrical and magnetic properties of ferrites can be tailored by controlling the different type and amount of metal ion substitution. Rare earth ions have unpaired 4f electrons that have a role to cause magnetic anisotropy due to their orbital shape. Introducing the Gd^{3+} ions into spinel lattice will lead to the appearance of 3d-4f couplings between transition metal and Gd^{3+} ions[15]; thus, the electrical and magnetic properties of ferrite can be improved.

It is known that the conducting materials can effectively shield electromagnetic waves generated from an electric source, whereas electromagnetic waves from a magnetic source, especially at low frequencies, can be effectively shielded only by magnetic materials. Thus, fabrication of the conducting PANI-magnetic ferrite composite used as EMI shielding materials, good shielding effectiveness, can be achieved for various electromagnetic sources. Up to date, preparation of PANI with ferromagnetic properties has been studied by Wan's group.[16,17] Deng et al. have studied the synthesis of magnetic and conducting Fe_3O_4-crosslinked PANI nanoparticles with core–shell structure by using precipitation–oxidation technique.[18] Yang et al. have reported the preparation of conducting and magnetic PAn/γ-Fe_2O_3 composite by modification–redoping method.[19] Recently, the fabrication of MnZn or NiZn ferrite-PANI composite has been reported.[20–22]

In this article, magnetic composite containing PANI-coated $LiNi_{0.5}Gd_{0.08}Fe_{1.92}O_4$ ferrite was synthesized by *in situ* polymerization of aniline on the sur-

Correspondence to: L. Li (sky52@zjnu.cn).
Contract grant sponsor: Top Key Discipline of Material Physics and Chemistry in Zhejiang Provincial Colleges, Zhejiang Provincial Natural Science Foundation of China; contract grant number: Y405038.

Journal of Applied Polymer Science, Vol. 105, 944–950 (2007)

face of ferrite particles obtained by the rheological phase reaction method.[23] The samples were characterized by various experimental techniques, and the magnetic properties of composite were investigated.

EXPERIMENTAL

Materials

Aniline monomer was distilled under reduced pressure and stored below 0°C. Ammonium peroxydisulfate ($(NH_4)_2S_2O_8$), ferric oxide (Fe_2O_3), lithium carbonate (Li_2CO_3), nickel sulfate ($NiSO_4{\cdot}6H_2O$), gadolinium oxide (Gd_2O_3), and oxalic acid ($H_2C_2O_4{\cdot}2H_2O$) were all analytical reagent grade and used as received. All reagents were purchased from Shanghai chemical agents in China.

Preparation of $LiNi_{0.5}Gd_{0.08}Fe_{1.92}O_4$ ferrite

The Gd-substituted LiNi ferrite ($LiNi_{0.5}Gd_{0.08}Fe_{1.92}O_4$) was prepared by the rheological phase reaction method. In a typical procedure, stoichiometric amounts of Li_2CO_3, $NiSO_4{\cdot}6H_2O$, Gd_2O_3, Fe_2O_3, and $H_2C_2O_4 \cdot 2H_2O$ were thoroughly mixed by grinding in an agate mortar for 30 min. About 35 mL ethanol was then added to form the mixture in rheological state. The mixture was sealed in a Teflon-lined, stainless-steel autoclave and maintained at 120°C for 48 h in an oven. The obtained precursor was washed several times with deionized water and ethanol, dried at 60°C for 12 h, and sintered at 1000°C for 2 h in air, followed by cooling in a furnace to room temperature at 5°C/min cooling rate.

Synthesis of PANI-$LiNi_{0.5}Gd_{0.08}Fe_{1.92}O_4$ composite

PANI-$LiNi_{0.5}Gd_{0.08}Fe_{1.92}O_4$ composite was prepared by *in situ* polymerization in aqueous solution of hydrochloric acid. In a typical procedure, 0.1 g (about 10% (w/w) weight ratio of ferrite to aniline) of $LiNi_{0.5}Gd_{0.08}Fe_{1.92}O_4$ particles was suspended in 35 mL of 0.1*M* HCl solution and stirred for 30 min. Then 1 mL of aniline monomer was added to the suspension and stirred for 30 min. $(NH_4)_2S_2O_8$ (2.49 g) in 20 mL of 0.1*M* HCl solution was then slowly added dropwise to the suspension mixture, with constant stirring. The polymerization was allowed to proceed for 12 h at room temperature. The composite was obtained by filtering and washing the suspension with 0.1*M* HCl and deionized water, and dried under vacuum at 60°C for 24 h.

Methods and instrumentation

X-ray diffraction (XRD) patterns were collected on a Philps-PW3040/60 diffractometer with Cu Kα radiation ($\lambda = 0.15418$ nm). The morphology and particle sizes of samples were determined on a Hitachi H-800 transmission electron microscope (TEM) with an accelerating voltage of 200 kV. FTIR spectra were recorded on a Nicolet Nexus 670 spectrometer in the range of 400–2000 cm^{-1} using KBr pellets. UV–vis absorption spectra were recorded on a Shimadzu UV-2501PC spectrophotometer in the range of 300–800 nm. *N*,*N*-Dimethylformamide was used as a solvent to prepare the sample solution. Thermogravimetric analysis (TGA) measurements were carried out using a Shimadzu TGA-50 thermogravimetric analyzer in an alumina crucible with alumina as reference sample, at a heating rate of 10°C/min and a flow rate of 40 mL/min in air atmosphere. Magnetic measurements were carried out at room temperature using a vibrating sample magnetometer (Lakeshore 7403) under applied magnetic field.

RESULTS AND DISCUSSION

XRD analysis

Figure 1 shows XRD patterns of $LiNi_{0.5}Gd_{0.08}Fe_{1.92}O_4$ ferrite, PANI, and PANI-$LiNi_{0.5}Gd_{0.08}Fe_{1.92}O_4$ composite. $LiNi_{0.5}Gd_{0.08}Fe_{1.92}O_4$ [Fig. 1(a)] shows the characteristic peaks at $2\theta = 18.44°$, 30.14°, 35.66°, 37.13°, 43.22°, 53.75°, 57.16°, and 62.81°, with the reflection of *Fd3m* cubic spinel group, which indicates the formation of the single spinel phase. The typical XRD pattern of PANI is given in Figure 1(c), which shows two broad diffraction peaks at $2\theta = 20.21°$ and 25.39°, indicating that HCl-doped PANI has some degree of crystallinity. Both broad peaks may ascribe to the periodicity parallel to the polymer chain.[24,25] The diffraction peaks for the PANI-$LiNi_{0.5}Gd_{0.08}Fe_{1.92}O_4$ composite in Figure 1(b) exhibit both the characteristic peaks of the $LiNi_{0.5}Gd_{0.08}Fe_{1.92}O_4$ ferrite and the broad diffraction peaks of PANI, and the in-

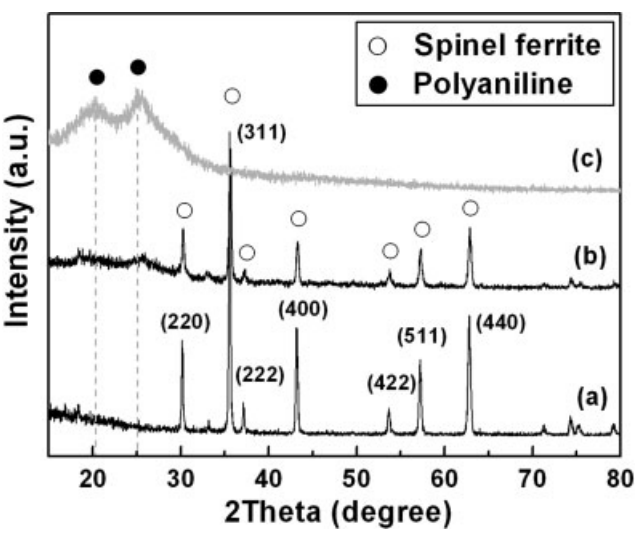

Figure 1 XRD patterns of $LiNi_{0.5}Gd_{0.08}Fe_{1.92}O_4$ (a), PANI-$LiNi_{0.5}Gd_{0.08}Fe_{1.92}O_4$ composite (b), and PANI (c).

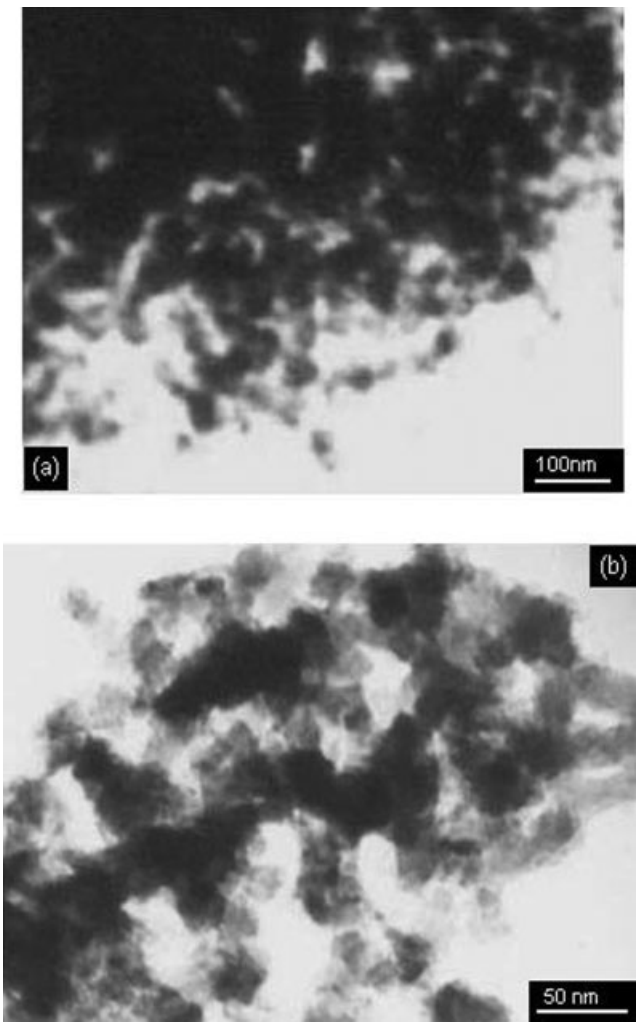

Figure 2 TEM images of $LiNi_{0.5}Gd_{0.08}Fe_{1.92}O_4$ (a) and PANI-$LiNi_{0.5}Gd_{0.08}Fe_{1.92}O_4$ composite (b).

tensity of peaks for the composite is weaker than that of the pure ferrite, which reveals the formation of the PANI-$LiNi_{0.5}Gd_{0.08}Fe_{1.92}O_4$ composite.

The average crystallite sizes of PANI-$LiNi_{0.5}Gd_{0.08}Fe_{1.92}O_4$ composite can be calculated by the Debye–Scherrer formula[26]

$$\beta = \frac{k\lambda}{D\cos\theta} \quad (1)$$

where λ is the X-ray wavelength (0.15418 nm), k is the shape factor taken as 0.89, D is the average size of the crystals, θ is the Bragg's angle, and β is FWHM of the strongest diffraction peak. The average crystallite sizes of the composite particles are 64.2 nm, which is consistent with the results detected by TEM.

Morphology

The morphology and particle sizes of $LiNi_{0.5}Gd_{0.08}Fe_{1.92}O_4$ and PANI-$LiNi_{0.5}Gd_{0.08}Fe_{1.92}O_4$ composite were observed by TEM. Figure 2(a) shows the TEM image of the $LiNi_{0.5}Gd_{0.08}Fe_{1.92}O_4$ ferrite particles. The average size of the $LiNi_{0.5}Gd_{0.08}Fe_{1.92}O_4$ particles is estimated to be in the range of 50–70 nm, but having agglomeration to some extent, because of the high surface energy of the nanoparticles. It is clearly seen from Figure 2(b) that the inner dark core of $LiNi_{0.5}Gd_{0.08}Fe_{1.92}O_4$ is spherical or elliptical, and the gray shell of PANI is enwrapped loosely on the $LiNi_{0.5}Gd_{0.08}Fe_{1.92}O_4$ particles, forming the core–shell structure of PANI-$LiNi_{0.5}Gd_{0.08}Fe_{1.92}O_4$ composite.

Fourier transform infrared spectra analysis

Figure 3 shows the Fourier transform infrared spectra (FTIR) spectra of the $LiNi_{0.5}Gd_{0.08}Fe_{1.92}O_4$, PANI, and PANI-$LiNi_{0.5}Gd_{0.08}Fe_{1.92}O_4$ composites. In ferrites, the metal ions are situated in two different sublattices, designated as tetrahedral and octahedral according to the geometrical configuration of the oxygen nearest neighbors. Waldron[27] and Hafner[28] studied the vibrational spectra of ferrite, and attributed high frequency band ν_1 (600–580 cm^{-1}) to the intrinsic vibration of the tetrahedral sites and low frequency band ν_2 (440–410 cm^{-1}) to the intrinsic vibration of the octahedral site. It is observed from the IR spectrum of the $LiNi_{0.5}Gd_{0.08}Fe_{1.92}O_4$ that the peaks at 589 and 418 cm^{-1} are intrinsic vibration of the tetrahedral and octahedral sites, respectively.

The characteristic peaks of PANI occur at 1577, 1494, 1301, 1240, 1139, and 805 cm^{-1}. The peaks at 1577 and 1494 cm^{-1} are attributed to the characteristic C=C stretching of the quinoid and benzenoid rings,[29,30] the peaks at 1301 and 1240 cm^{-1} are assigned to C—N stretching of the benzenoid ring,[31] the broad peak at 1139 cm^{-1} which is described by MacDiarmid et al. as the ''electronic-like band'' is associated with vibration mode of N=Q=N, indicat-

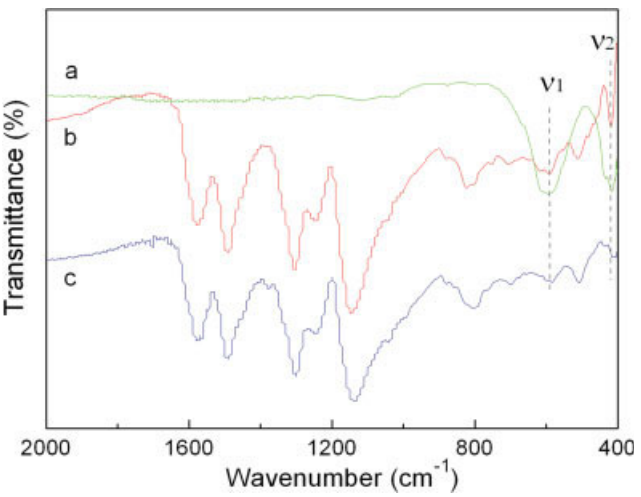

Figure 3 FTIR spectra of $LiNi_{0.5}Gd_{0.08}Fe_{1.92}O_4$ (a), PANI-$LiNi_{0.5}Gd_{0.08}Fe_{1.92}O_4$ composite (b), and PANI (c). [Color figure can be viewed in the online issue, which is available at www.interscience.wiley.com.]

TABLE I
Assignment of FTIR Absorption Peaks for PANI and PANI-$LiNi_{0.5}Gd_{0.08}Fe_{1.92}O_4$ Composite

Wavenumber (cm^{-1})		
PANI	PANI-$LiNi_{0.5}Gd_{0.08}Fe_{1.92}O_4$ composite	Peak assignment
1577	1576	Quinoid ring stretching band
1494	1493	Benzenoid ring stretching band
1301, 1240	1304, 1247	Aromatic C—N stretching band
1139	1145	C—H in-plane bending vibration
804	812	p-disubstituted aromatic ring
–	589	Vibration of the tetrahedral site (ν_1)
–	418	Vibration of the octahedral site (ν_2)

ing that HCl-doped PANI is formed in our samples,[32] and the peak at 805 cm^{-1} is attributed to the out-of-plane deformation of C—H in the p-disubstituted benzene ring.[33] It is seen from Figure 3(b) that the IR spectrum of PANI-$LiNi_{0.5}Gd_{0.08}Fe_{1.92}O_4$ composite is similar to that of PANI, and the characteristic peaks of $LiNi_{0.5}Gd_{0.08}Fe_{1.92}O_4$ at 589 and 418 cm^{-1} can be found in the spectrum of the composite. However, the peaks at 1301, 1240, and 1139 cm^{-1} corresponding to PANI characteristics shift to higher wave numbers (Table I). These results indicate that there is an interaction between $LiNi_{0.5}Gd_{0.08}Fe_{1.92}O_4$ ferrite particles and PANI.[34]

UV–vis spectra analysis

Figure 4 gives UV–vis absorption spectra of PANI and PANI-$LiNi_{0.5}Gd_{0.08}Fe_{1.92}O_4$ composite. It is observed from Figure 4(a) that the PANI has two characteristic absorption bands at around 329 and 617 nm. The absorption band around 329 nm is attributed to π-π* transition of the benzenoid ring,[35,36] while the peak around 617 nm corresponds to the benzenoid-to-quinoid excitonic transition.[37,38] It is found from Figure 4(b) that the absorption peaks of PANI-$LiNi_{0.5}Gd_{0.08}Fe_{1.92}O_4$ ferrite composite have a red shift of 3 and 5 nm, respectively, when compared with that of PANI. This result may indicate that the interaction appears between ferrite particles and PANI backbone, which may make the energy of antibonding orbital to decrease, leading to the energy of the π-π* transition of the benzenoid and quinoid ring to decrease, and consequently the absorption peaks of composite exhibit a red shift.

TGA analysis

Thermal behavior of PANI and PANI-$LiNi_{0.5}Gd_{0.08}Fe_{1.92}O_4$ composite is investigated through TGA. Figure 5 shows the typical TGA curves of PANI and PANI-$LiNi_{0.5}Gd_{0.08}Fe_{1.92}O_4$ composite. The TG curve of PANI presents the two major steps of weight loss (DTG peaks at 91.2°C and 418.7°C), and indicates that the decomposition is complete at around 680°C. The first-step corresponds to a weight loss of about 4% and can be attributed to the release of water molecules. The second-step indicates a weight loss of

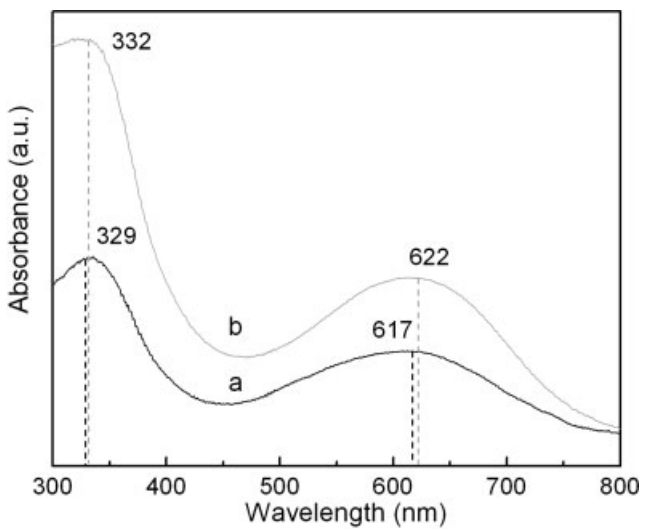

Figure 4 UV–vis spectra of PANI (a) and PANI-$LiNi_{0.5}Gd_{0.08}Fe_{1.92}O_4$ composite (b).

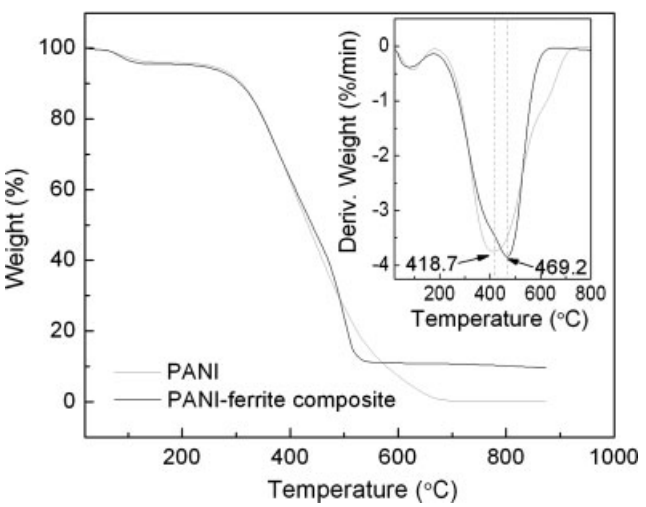

Figure 5 TGA curves and DTG curves (inset) of PANI and PANI-$LiNi_{0.5}Gd_{0.08}Fe_{1.92}O_4$ composite.

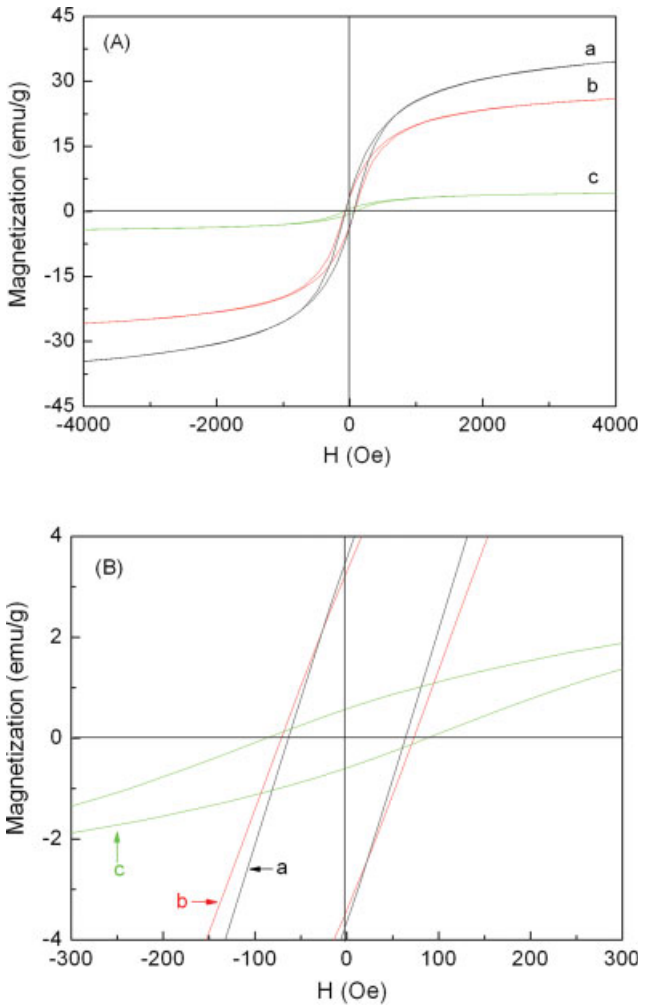

Figure 6 Magnetic hysteresis loops of $LiNi_{0.5}Fe_2O_4$ (a), $LiNi_{0.5}Gd_{0.08}Fe_{1.92}O_4$ (b), and PANI-$LiNi_{0.5}Gd_{0.08}Fe_{1.92}O_4$ composite (c) with (A) a magnetic field of 4000 Oe and (B) a low field range. [Color figure can be viewed in the online issue, which is available at www.interscience.wiley.com.]

about 94%, which is ascribed to the degradation of the polymer chains. The trend of degradation for PANI-$LiNi_{0.5}Gd_{0.08}Fe_{1.92}O_4$ composite is similar to that of PANI. The TGA curve of PANI-$LiNi_{0.5}Gd_{0.08}Fe_{1.92}O_4$ composite also presents two-step weight loss process, and shows that the decomposition of PANI-$LiNi_{0.5}Gd_{0.08}Fe_{1.92}O_4$ composite is complete at around 560°C. DTG curves are shown in the inset of Figure 5 to compare the thermal behavior of PANI with that of PANI-$LiNi_{0.5}Gd_{0.08}Fe_{1.92}O_4$ composite. The peak temperature on the DTG curves indicates that the reaction rate is highest at this point. It is seen clearly that the temperature of PANI at the minimum of the DTG curve is at 418.7°C, while the minimum temperature in the case of PANI-$LiNi_{0.5}Gd_{0.08}Fe_{1.92}O_4$ composite is significantly shifted to a higher temperature (469.2°C), which is in agreement with the results of Wang et al.[39]

Magnetic properties

Figure 6 shows the magnetic hysteresis loops of LiNi ferrite ($LiNi_{0.5}Fe_2O_4$), Gd-subsitituted LiNi ferrite ($LiNi_{0.5}Gd_{0.08}Fe_{1.92}O_4$), and PANI-$LiNi_{0.5}Gd_{0.08}Fe_{1.92}O_4$ composite at room temperature. The magnetization under applied magnetic field for the as-prepared samples exhibits a clear hysteretic behavior. In a ferrimagnet, the magnetic moments of tetrahedral A-sites and octahedral B-sites are aligned antiparallel and are not equal, because of antiferromagnetic coupling, resulting in a finite difference to yield a net magnetization ($m = m_B - m_A$). In general, Li^+, Ni^{2+}, and Gd^{3+} ions preferably enter octahedral B-sites.[40,41] The magnetic moments of rare-earth ions generally originate from localized 4f electrons and they are characterized by lower magnetic ordering temperatures, i.e., lower than 40 K,[42] and their magnetic dipolar orientation exhibits disordered form at room temperature. Hence, it may be reasonable that Gd^{3+} ions are considered as nonmagnetic ions. The observed decrease in magnetization with substituting Gd^{3+} ions is due to the dilution of magnetization of B-sublattice by Gd^{3+} ions, whereas the increase in coercivity of Gd-subsitituted LiNi ferrite can be considered in that the larger Gd^{3+} replacing for Fe^{3+} at B-sites may induce some distortion in the spinel lattice leading to larger internal stress.

The magnetic parameters such as saturation magnetization (M_S) and coercivity (H_C) of $LiNi_{0.5}Fe_2O_4$, $LiNi_{0.5}Gd_{0.8}Fe_{1.92}O_4$, and PANI-$LiNi_{0.5}Gd_{0.08}Fe_{1.92}O_4$ determined by hysteresis loops are given in Table II. There is a decrease in M_S while an increase in H_C for PANI-$LiNi_{0.5}Gd_{0.08}Fe_{1.92}O_4$ composite was compared with that of $LiNi_{0.5}Gd_{0.08}Fe_{1.92}O_4$ ferrite. According to the equation $M_S = \varphi m_S$, M_S is related to the volume fraction of the particles (φ) and the saturation moment of a single particle (m_S).[43] It is considered that the saturation magnetization of PANI-$LiNi_{0.5}Gd_{0.08}Fe_{1.92}O_4$ composite depends mainly on the volume fraction of the magnetic ferrite particles, because of the nonmagnetic PANI coating layer contribution to the total magnetization, resulting in a decrease in the saturation magnetization. The coercivity of PANI-$LiNi_{0.5}Gd_{0.08}Fe_{1.92}O_4$ composite in this study presents a higher value than that of $LiNi_{0.5}Gd_{0.08}Fe_{1.92}O_4$ ferrite. It is known that the coercivity is related to the microstructure, magnetic anisotropy

TABLE II
Magnetic Parameters of $LiNi_{0.5}Fe_2O_4$, $LiNi_{0.5}Gd_{0.08}Fe_{1.92}O_4$, and PANI-$LiNi_{0.5}Gd_{0.08}Fe_{1.92}O_4$ Composite

Sample	M_S (emu/g)	H_C (Oe)
$LiNi_{0.5}Fe_2O_4$	34.44	63.11
$LiNi_{0.5}Gd_{0.08}Fe_{1.92}O_4$	26.55	70.45
PANI-$LiNi_{0.5}Gd_{0.08}Fe_{1.92}O_4$ composite	4.37	83.69

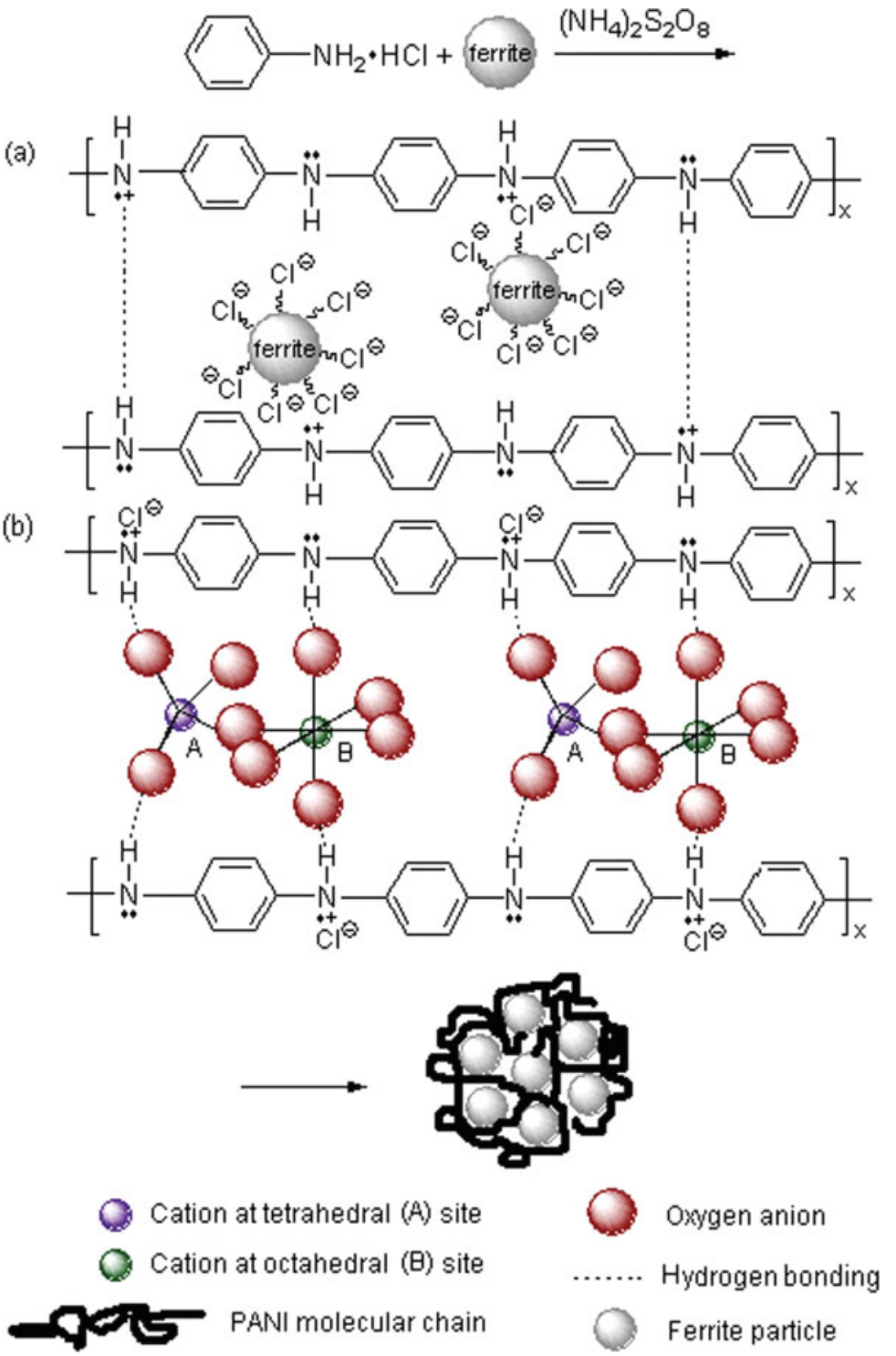

Figure 7 Bonding mechanism in the composite: charge compensation mechanism (a) and hydrogen bonding mechanism (b). [Color figure can be viewed in the online issue, which is available at www.interscience.wiley.com.]

(crystal, stress, and shape), and magnetorestriction of magnetic ferrite particles. The anisotropy and magnetorestriction are dependent on factors like composition, imperfections, porosity, crystalline shape, etc. Polycrystalline ferrites have an irregular structure, geometric and crystallographic nature, such as pores, cracks, surface roughness, and impurities. In the polymerization process, PANI is deposited on the ferrite surface and crystallite boundary, which may lead to an increase in magnetic surface anisotropy of ferrite particles. On the other hand, there is a possible charge transfer between the ferrite surface and PANI chains.

This interaction may change the electron density at the ferrite surfaces and, thus, affect the processes of electron spins in the system, resulting in the increase of spin–orbit couplings at the surface of ferrite particles.

Bonding interactions

Bonding interactions between ferrite and PANI backbone in the composite are illustrated in Figure 7. We propose the probable bonding mechanism in the composite according to the results of spectroanalysis. Figure 7(a) shows the charge compensation mechanism in the composite. The surface of the ferrite is positively charged due to the polymerization in the acidic environment. Therefore, adsorption of an amount of the Cl^- may compensate the positive charges on ferrite surface. Beside this charge compensation process, specific adsorption of the Cl^- on the ferrite surface would work as the charge compensator for protonated PANI chain in the formation of PANI-ferrite composite. There is charge compensation effect between ferrites and PANI chains in the composite.

Another bonding mechanism may be hydrogen bonding in the composite, as shown in Figure 7(b). In the aqueous solution of hydrochloric acid, some oxygen atoms located at tetrahedral and octahedral sublattices may expose on the surface of the ferrite, and have the tendency to accept proton, resulting in occurrence of the hydrogen bonding between the oxygen atoms and PANI chains in the composite. In addition, hydrogen bonding between PANI chains may also exist in the composite.

CONCLUSIONS

PANI-$LiNi_{0.5}Gd_{0.08}Fe_{1.92}O_4$ composite with the core–shell structure presenting ferromagnetic behavior was successfully synthesized by *in situ* polymerization of aniline in the presence of ferrite particles. FTIR and UV–vis spectra indicated that there was an interaction between PANI and $LiNi_{0.5}Gd_{0.08}Fe_{1.92}O_4$ ferrite in the composite. XRD diffraction patterns demonstrated the formation of PANI-$LiNi_{0.5}Gd_{0.08}Fe_{1.92}O_4$ composite. The composite exhibited the intrinsic magnetic hysteresis of the ferrite particles. Bonding interaction between PANI and $LiNi_{0.5}Gd_{0.08}Fe_{1.92}O_4$ ferrite in composite was discussed.

References

1. Mäkelä, T.; Pienimaa, S.; Taka, T.; Jussila, S.; Isotalo, H. Synth Met 1997, 85, 1335.
2. Kuwabata, S.; Masui, S.; Yoneyama, H. Electrochim Acta 1999, 44, 4593.
3. Kan, J. Q.; Pan, X. H.; Chen, C. Biosens Bioelectron 2004, 19, 1635.
4. Ahmad, N.; MacDiarmid, A. G. Synth Met 1996, 78, 103.
5. Rose, T. L.; Antonio, S. D.; Jillson, M. H.; Kron, A. B.; Suresh, R.; Wang, F. Synth Met 1997, 85, 1439.
6. Danielle, C.; Michelle, S.; Ivo, A.; Aldo, Z. Chem Mater 2003, 15, 4658.
7. Qiu, Y.; Gao, L. J Phys Chem B 2005, 109, 19732.
8. Han, J.; Song, G.; Guo, R. J Polym Sci Part A: Polym Chem 2006, 44, 4229.
9. Khiew, P. S.; Huang, N. M.; Radiman, S.; Ahmad, S. M. Mater Lett 2004, 58, 516.
10. Qiu, Y.; Gao, L. J Phys Chem B 2005, 109, 19732.
11. Feng, X.; Mao, C.; Yang, G.; Hou, W.; Zhu, J. J. Langmuir 2006, 22, 4384.
12. Yoshimoto, S.; Ohashi, F.; Kameyama, T. J Polym Sci Part B: Polym Phys 2005, 43, 2705.
13. Schloeman, E. J Magn Magn Mater 2000, 209, 15.
14. Pardavi-Horvath, M. J Magn Magn Mater 2000, 215–216, 171.
15. Kahn, M. K.; Zhang, Z. J Appl Phys Lett 2001, 78, 3651.
16. Wan, M. X.; Li, W. C. J Polym Sci Part A: Polym Chem 1997, 34, 2129.
17. Wan, M. X.; Fan, J. H. J Polym Sci Part A: Polym Chem 1998, 36, 2749.
18. Deng, J.; Ding, X.; Zhang, W.; Peng, Y.; Wang, J.; Long, X.; Li, P.; Chan, A. S. C. Polymer 2002, 43, 2179.
19. Yang, Q. L.; Zhai, J.; Feng, L.; Song, Y. L.; Wan, M. X.; Jiang, L.; Xu, W. G.; Li, Q. S. Synth Met 2003, 135–136, 819.
20. Kazantseva, N. E.; Vilcáková, J.; Kěsálek, V.; Sáha, P.; Sapurina, I.; Stejskald, J. J Magn Magn Mater 2004, 269, 30.
21. Yavuz, Ö.; Ram, M. K.; Aldissi, M.; Poddar, P.; Hariharan, S. J Mater Chem 2005, 15, 810.
22. Li, G.; Yan, S.; Zhou, E.; Chen, Y. Colloids Surf A 2006, 276, 40.
23. Diakite, K.; Zhan, D.; Zhang, K. Mater Lett 2005, 59, 2243.
24. Moon, Y. B.; Cao, Y.; Smith, P.; Heeger, A. J. Polym Commun 1989, 30, 196.
25. Feng, W.; Sun, E.; Fujii, A.; Wu, H. C.; Niihara, K.; Yoshino, K. Bull Chem Soc Jpn 2000, 73, 2627.
26. Klug, H. P.; Alexander, L. E. X-ray Diffraction Procedures for Polycrystalline and Amorphous Materials; Wiley: New York, 1954.
27. Waldron, R. D. Phys Rev 1955, 99, 1727.
28. Hafner, S. R. Z Kristallogr 1961, 115, 331.
29. Wei, Z.; Zhang, Z.; Wan, M. Langmuir 2002, 12, 897.
30. Du, J.; Liu, Z.; Han, B.; Li, Z.; Zhang, J.; Huang, Y. Micropor Mesopor Mat 2005, 84, 254.
31. Li, C. C.; Zhang, Z. K. Macromolecules 2004, 37, 2683.
32. Quillard, S.; Louarn, G.; Lefrant, S.; MacDiarmid, A. G. Phys Rev B 1994, 50, 12496.
33. Kulkarni, M. V.; Viswanath, A. K.; Marimuthu, R.; Seth, T. Polym Eng Sci 2004, 44, 1676.
34. Li, X.; Wang, G.; Li, X.; Lu, D. Appl Surf Sci 2004, 229, 395.
35. Epstein, A. J; Ginder, J. M.; Zuo, F.; Bigelow, R. W.; Woo, H. S.; Tanner, D. B.; Richter, A. F.; Huang, W. S.; MacDiaarmid, A.G. Synth Met 1987, 18, 303.
36. Wan, M. X. Synth Met 1989, 31, 51.
37. Venugopal, G.; Quan, X.; Johnson, G. E.; Houlihan, F. M.; Chin, E.; Nalamasu, O. Chem Mater 1995, 7, 271.
38. Gruger, A.; Novak, A.; Regis, A.; Colomban, P. J Mol Struct 1994, 328, 153.
39. Wang, S.; Tan, Z.; Li, Y.; Sun, L.; Zhang, T. Thermochim Acta 2006, 441, 191.
40. Li, Y. Y.; Li, G. D.; Ferrite Physics; Science Press: Beijing, 1974.
41. Sattar, A. A.; El-Shokrofy, K. M. J. Phys IV 1997, C1, 245.
42. Nellis, W. J.; Legvold, S. Phys Rev 1969, 180, 581.
43. Sauzedde, F.; Elaissari, A.; Pichot, C. Colloid Polym Sci 1999, 277, 846.